inorganics

MDPI

Article

Protonic Kenyaite and Its Removal Performance of Basic Blue-41: Comparative Study, Operational Conditions and Regeneration Studies

Rawan Al-Faze [1], Mohd Gulfam Alam [2], Thamer S. Alraddadi [2], Saheed A. Popoola [2,*], Souad Rakass [3], Hicham Oudghiri Hassani [4], Abdulganiyu O. Logunleko [5] and Fethi Kooli [2,*]

1 Department of Chemistry, Faculty of Science, Taibah University, Madinah 30002, Saudi Arabia; rafaze@taibahu.edu.sa
2 Department of Chemistry, Faculty of Science, Islamic University of Madinah, Madinah 42351, Saudi Arabia; gulfam@iu.edu.sa (M.G.A.); talraddadi@iu.edu.sa (T.S.A.)
3 Laboratory of Applied Organic Chemistry (LCOA), Chemistry Department, Faculty of Sciences and Techniques, Sidi Mohamed Ben Abdellah University, Imouzzer Road, P.O. Box 2202, Fez 30000, Morocco; souad.rakass@usmba.ac.ma
4 Engineering Laboratory of Organometallic, Molecular Materials, and Environment (LIMOME), Faculty of Sciences, Chemistry Department, Sidi Mohamed Ben Abdellah University, P.O. Box 1796, Fez 30000, Morocco; hicham.oudghirihassani@usmba.ac.ma
5 Department of Chemistry, Sikiru Adetona College of Education, Science and Technology, Omu Ajose, Ijebu Ode PMB 2128, Ogun State, Nigeria; logunlekoao@sacoetec.edu.ng
* Correspondence: abiodun@iu.edu.sa (S.A.P.); fethi_kooli@yahoo.com (F.K.)

Abstract

The discharge of cationic dyes such as Basic Blue-41 (BB-41) into natural water bodies remains a major environmental concern. Herein, the efficiency of protonated kenyaite (H-Knt) for BB-41 removal from aqueous solution was investigated and compared to Na-kenyaite (Na-Knt). H-Knt exhibited a basal spacing of 1.60 nm, smaller than that of Na-Knt (1.92 nm), confirming the exchange of interlayer Na cations with protons. ^{29}Si MAS NMR analysis revealed structural disorder within the silicate layers, particularly at the Q^4 Si sites, along with an increase in surface area from 29.6 m^2/g to 38.4 m^2/g. Linear and non-linear fitting using the Langmuir, Freundlich, and Sips isotherm models were performed to estimate the maximum removal capacity (q_{max}) of the tested materials. The removal efficiency of BB-41 increased under alkaline conditions. H-Knt showed a removal capacity of 61 mg/g (from non-linear Langmuir model). Kinetic studies demonstrated that the pseudo-second-order model provided the best fit to the experimental data. The regeneration performance of H-Knt was evaluated for seven consecutive cycles, during which its removal efficiency decreased by up to 30%. Finally, a single-batch adsorber system was theoretically designed to estimate the required masses of Na-Knt and H-Knt needed to achieve BB-41 removal efficiencies ranging from 50% to 95%.

Keywords: Na-kenyaite; protonic-kenyaite; Basic Blue-41; removal; regeneration; single batch design

Check for updates

Academic Editor: Antonino Gulino

Received: 30 September 2026
Revised: 9 November 2026
Accepted: 12 November 2026
Published: 15 November 2026

Copyright: © 2026 by the authors. Licensee MDPI, Basel, Switzerland. This article is an open access article distributed under the terms and conditions of the Creative Commons Attribution (CC BY) license.

1. Introduction

The textile industry is one of the largest consumers of water and a major source of wastewater generation. Moreover, the discharge of untreated effluents into waterways alters aquatic ecosystems and exerts profound environmental impacts, including oxygen depletion and biodiversity loss, by disturbing ecosystem balance [1]. Different methods have been

proposed for treating contaminated water, including physical, chemical, and biological approaches [2]. The selection of an appropriate method is determined by the characteristics of the wastewater, operational costs, and the ease of operation [2]. Considerable attention has been focused on the adsorption process. Several reviews have been published discussing this process in terms of operational simplicity, avoidance of added chemicals, and absence of undesirable by-products [3,4]. Adsorbents play a central role in this process because of their high surface areas and/or functional groups, resulting in strong affinity toward dye molecules and notable adsorption efficiency [5]. Natural abundance, harmlessness, cost-effectiveness, and reusability are major considerations when selecting a suitable adsorbent for water treatment [6–8]. Commercial activated carbon, as well as various low-cost adsorbents derived from natural materials, industrial solid wastes, agricultural by-products, and biosorbents, have been proposed for this purpose [9].

The aluminosilicate (clays) family has been extensively examined for the adsorption of pollutants, including metal cations, pharmaceuticals, and dyes [10–12]. Pure hydrous layered silicate materials, such as kenyaite (Na-Knt), have attracted a lot of attention. The interlayer space is lined with silanol (Si–OH) groups, which can generate stable negative charges through deprotonation [13]. These negative charges are crucial to the removal of cationic dyes. Na-Knt occurs naturally only in small amounts and in limited locations [14]. It is considered as nontoxic material and can be readily prepared in the laboratory under specific conditions, including the silica source, SiO_2/NaOH/H_2O molar ratio, temperature, and reaction time [15]. Compared with the wide range of applications of clay minerals, Na-Knt has been reported for use in catalysis [16], composites [17], zeolite precursors [18], and environmental remediation for the elimination of certain metals and organic pollutants [15,19–23].

The acid activation of aluminosilicates leads to a significant increase in surface area, typically by three- to fivefold, as well as improvements in pore volume and removal properties [24,25]. For Na-magadiite (Na-Mgd), another type of hydrous layered silicate, acid treatment produces its protonic form (H-Mgd), with a surface area of 30 m^2/g. However, its removal performance toward BB-41 and methylene blue (MB) was lower than that of the starting Na-Mgd sample [26,27]. This difference was attributed to the reduction in removal sites and the acidic nature of H-Mgd, which affected the final pH values of the dye solutions.

While previous investigations have explored the parent Na-kenyaite, Na and protonated magadiites, and various acid-activated aluminosilicates, the specific protonation of Na-kenyaite remains less explored. The present work provides an insight that interlayer of H-Knt shrank from 1.92 nm to 1.60 nm, and reduced considerably the BB-41 removal capacity due to an increase in the surface acidity. By directly comparing H-Knt with Na-Knt, this study elucidates how acid modification alters textural properties and removal performance, offering insights into the behavior of modified layered silicates during the dye removal and regeneration. The systematic treatment of Na-Knt with HCl solution and its specific effects on dye adsorption provide detailed data on changes in structure and texture, further defining the potential applications of these materials in environmental remediation. The starting Na-Knt and H-Knt samples were synthesized and characterized using different physicochemical techniques, including X-ray fluorescence (XRF), X-ray diffraction (XRD), thermogravimetric analysis (TGA), Fourier-transform infrared (FTIR), silicon-29 magic-angle spinning nuclear magnetic resonance (^{29}Si MAS NMR), scanning electron microscopy (SEM) associated with EDX, nitrogen (N_2) adsorption isotherms, and pH_{pzc} measurement. The removal properties of Na-Knt and H-Knt toward BB-41 dye were investigated. This dye was selected as a model because it is widely used in various industries, particularly the textile industry [28]. BB-41 is non-biodegradable, and its presence in water streams affects

human and animal health, as well as the stability of aquatic ecosystems [29]. Furthermore, the operational factors including pH, sample dosage, initial concentration, and contact time were systematically investigated. Isotherm data were fitted using Langmuir, Freundlich, and Sips models. Kinetic data were evaluated using pseudo-first-order (PFO), pseudo-second-order (PSO), and intra particle diffusion. More importantly, different isotherm models were used for the design of a single-batch adsorber. This design is used to predict the minimum masses of Na-Knt or H-Knt required to remove specific percentage of BB-41 from various volumes of a fixed initial concentration. This study also systematically examines the effectiveness of the regeneration process [15].

2. Results and Discussion

2.1. XRD Data

Figure 1A shows the powder XRD patterns of Na-Knt and its protonic H-Knt sample. Na-Knt exhibited a pattern comparable to those reported for the same material in the literature [19,30–32]. The pattern is also consistent with the reported pattern of Na-kenyaite (JCPDS card No: 20-1157) with a d_{001} of 1.92 nm and other multiple reflections. The position of the first reflection depends on the nature of the cations inserted between the kenyaite layers [32].

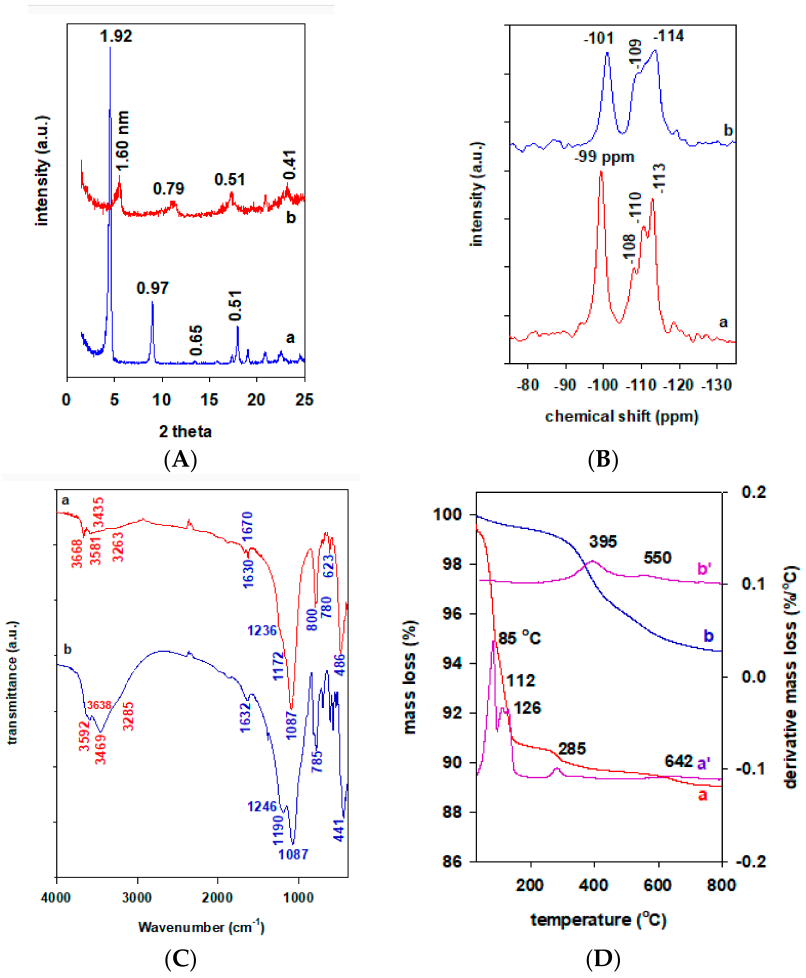


Figure 1. Characterization of (a) Na-Knt and (b) H-knt samples using different techniques. (**A**) PXRD, (**B**) FTIR, (**C**) ^{29}Si MAS NMR, and (**D**) TGA-DTG. (a) stands for Na-Knt and (b) stands for H-Knt samples.

After reaction with HCl solution, H-Knt exhibited a d_{001} reflection with an average value of 1.60 nm, as shown in Figure 1A. The reduction in the d_{001} value resulted from the exchange of Na cations with protons. In some cases, d_{001} values of 1.62 nm, 1.70 nm, and 1.80 nm have been reported for other protonated kenyaites [16,32,33]. This variation depends on the preparation methods. A decrease in intensity and the change in the shape of some reflections are related to the lower stacking order that occurred during HCl treatment. Similar observations have been reported for acid-activated clays [34]. During the acid treatment of Na-Knt, the crystallite size deduced from the Scherrer equation decreased from 70 nm to 51 nm.

The elemental analysis data of XRF and EDX confirmed a significant reduction in Na content in H-Knt sample. The calculated percentage was about 95% deduced from XRF data, and about 85% deduced from EDX technique (Table 1). The difference between the two techniques was attributed to the bulk-versus-surface analytical depth differences of the techniques. The results are consistent with proton exchange under the acid-treatment conditions.

Table 1. XRF, EDX, and thermogravimetric analysis (TGA) for Na-Knt and H-Knt samples.

Samples	Chemical Composition (wt, %)					TGA (%)
	SiO_2 [a]	Na_2O [a]	O [b]	Si [b]	Na [b]	H_2O [c]
Na-Knt	87.9	6.6	54.4	39.1	3.47	6.5
H-Knt	94.2	0.32	58.4	41.2	0.55	1.1

[a] XRF data, [b] EDX data, [c] TGA data.

2.2. ^{29}Si MAS NMR Analysis

The ^{29}Si MAS NMR technique was used to monitor changes in the silicon environment during the reaction with HCl solution. The Na-Knt spectrum showed four resonance peaks including triplet at −108 ppm, −110 ppm, and −113 ppm, associated with the presence of Si species in different Q^4 environments, and one intense peak at −99 ppm assigned to Q^3 sites, corresponding to silicon atoms in Q^3 [$Si(OSi)_3(OR)$] units, where R is either H or Na (Figure 1B). Comparable spectra have been reported for other Na-kenyaites [15,35]. After deconvolution of these bands, as shown in Figure S1, the Q^4/Q^3 ratio was estimated to be 1.52, which is lower than the values reported in the literature, where ratios of 3–4 have been mentioned [30,35,36]. These data indicate that the comparison of these ratios depends on the synthesis conditions and the measurement parameters.

After reaction with HCl solution, the ^{29}Si MAS NMR spectrum of H-Knt differed from that of Na-Knt (Figure 1B). The bands associated with Q^4 sites increased in intensity and became broader, with two bands observed at −109 and −114 ppm. Conversely, the intensity of the Q^3 band decreased, with a slight shift to −101 ppm [31]. The shifts in the Q^4 and Q^3 positions may be attributed to the stacking arrangement of the silicate layers and minor variations in the Si–O–Si angles. Comparable results have been reported for other hydrous layered silicates [26]. The Q^4/Q^3 ratio of H-Knt, estimated from the deconvolution of these bands (Figure S2), was 2.5. This value was lower than those reported in previous studies [26], which may be related to differences in the synthesis and acid-treatment conditions.

2.3. FTIR Analysis

FTIR spectroscopy was employed to investigate the structural changes in the Na-Knt after HCl treatment. The FTIR spectrum of Na-Knt (shown in Figure 1C) was comparable to that reported in the literature [37]. The OH stretching vibrations of water molecules and interlayer isolated silanol groups were identified at 3668, 3581, and 3435 cm^{-1}, respectively.

The deconvolution analysis revealed the presence of an additional broad band at 3263 cm^{-1} (Figure S3). The presence of water molecules was further confirmed by two bands at 1630 cm^{-1} and 1670 cm^{-1} [38].

The silicate framework gave rise to several bands in the range of 1450–860 cm^{-1}, including two broad bands at 1172 cm^{-1} and 1236 cm^{-1} and an intense band at 1087 cm^{-1}, which were assigned to Si–O–Si asymmetric stretching vibrations (Figure S4). The latter band was attributed to a class of materials containing five-membered rings in their structure [39]. Meanwhile, the Si–O–Si symmetric stretching modes were associated with a broad band at 690 cm^{-1} and two sharp bands at 800 and 782 cm^{-1}. The distinct bands detected at 623 cm^{-1} and 480 cm^{-1} were attributed to Si–O–Si bending deformations of the sample and double rings, respectively. In some cases, the band recorded at 782 cm^{-1} could be assigned to siloxide groups (–Si–O–, Na+) in the interlayer space. The appearance of the strong band at 486 cm^{-1} suggests that the kenyaite structure may also contain six-membered rings, in good agreement with the reported structure of Na-kenyaite [35].

The FTIR spectrum of H-Knt is presented in Figure 1C. The vibrations associated with hydration water around Na^+ cations and hydrogen bonding between free water molecules and Si–OH groups, observed at 1670 cm^{-1} and 1630 cm^{-1}, decreased in intensity due to the exchange of Na cations with protons. The bands at 3668 and 3581 cm^{-1} also decreased in intensity, while an enhancement of the silanol stretching band at 3442 cm^{-1} was observed (Figure S5) [39]. An intense band at 1078 cm^{-1} was clearly observed and assigned to Si–O terminal stretching. In addition, two bands at 1246 cm^{-1} and 1190 cm^{-1} were detected and assigned to the asymmetric stretching mode of Si–O–Si bonds. The sharp bands at 800 and 782 cm^{-1} were no longer observed [40]. These results indicate structural changes in the silicate framework during HCl treatment (Figure S6).

2.4. TGA and DTG Analysis

The TGA and derivative thermogravimetry (DTG) profiles of the Na-Knt and H-Knt samples are presented in Figure 1D. Na-Knt exhibited a mass loss of 5.7% between 25 °C and 80 °C, which was attributed to the removal of physiosorbed water molecules. In contrast, the loss of intercalated water bound to Na cations in the interlayer spacing (6.5%) occurred at relatively higher temperatures between 80 °C and 160 °C. Three DTG peaks were observed at 85 °C, 112 °C, and 126 °C, respectively (Figure 1D). Dihydroxylation of the silicate layers occurred at temperatures above 300 °C, with a mass loss of 0.77% associated with a DTG peak at 280 °C, as reported in previous studies [16,37,38].

Treatment of Na-Knt with HCl solution induced significant changes in the TGA features (Figure 1D). The two mass-loss steps observed for Na-Knt in the range of 25–180 °C were absent in H-Knt, confirming the removal of Na cations and their exchange with protons. In addition, no DTG peaks were recorded in this temperature range [26]. The loss of hydroxyl groups occurred at temperatures above 300 °C and was associated with two broad DTG peaks at 396 °C and 550 °C. The residual masses between 25 °C and 800 °C were 89.04% for Na-Knt and 94.07% for H-Knt, respectively.

2.5. SEM Examination

The morphological examination was carried out using SEM. According to the literature, Na-Knt can exhibit a rosette-like structure similar to that of Na-Mgd [19,38,40]. However, in the present study, a rosette-like structure was not observed. Instead, a stacked-plate morphology with different shapes and orientations was detected (Figure 2). The difference was associated with the synthesis conditions and the used chemicals. After reaction with HCl solution, the morphology of H-Knt was not significantly altered, although some disorder in

the stacking was observed, as reported for similar layered silicates (Figure 2) [16]. After BB-41 removal, SEM examination indicated slight morphological changes in both samples.

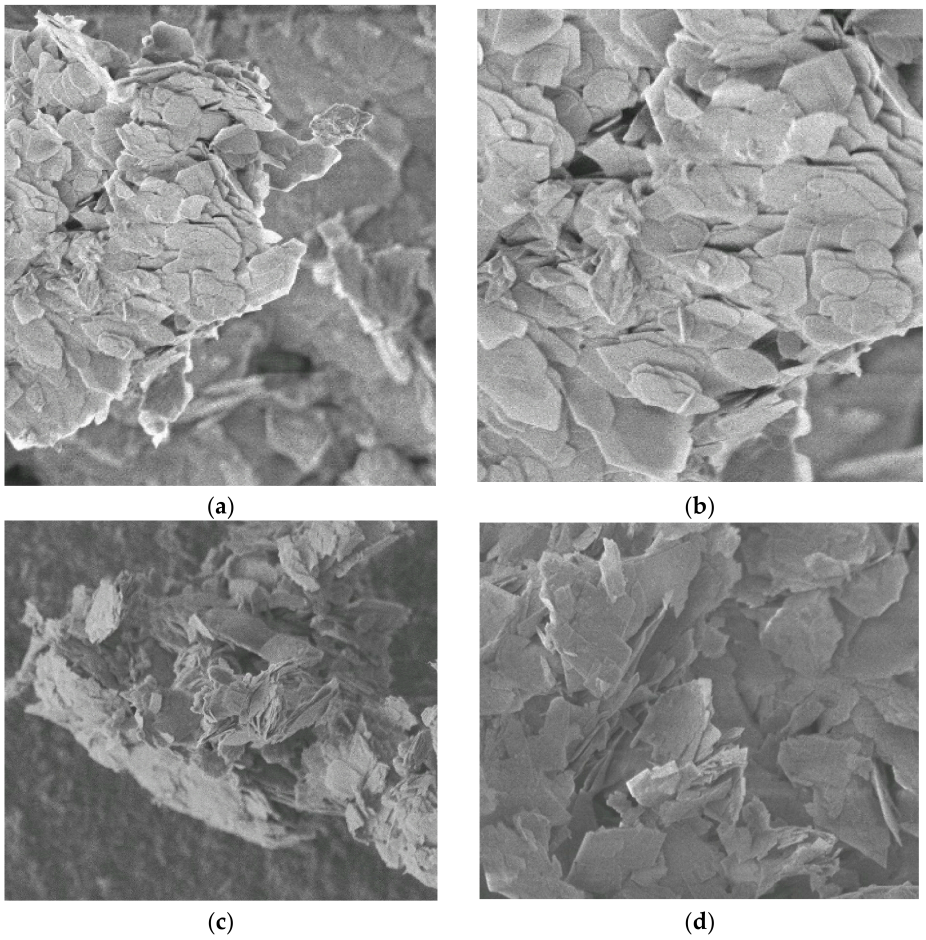


Figure 2. SEM micrographs of (**a**,**b**) Na-Knt and (**c**,**d**) H-Knt samples with magnification ×5000 for (**a**,**c**) and ×10,000 for (**b**,**d**), respectively.

2.6. Textural Properties

Table 2 summarizes the textural characteristics of Na-Knt and H-Knt. Na-Knt exhibits a type IV isotherm, characteristic of a mesoporous material, with a specific surface area (S_{BET}) of 29 m^2/g. Hydrous layered silicates usually exhibit surface areas ranging from 11 m^2/g to 49 m^2/g [21,22,27,30]. These values are influenced by the synthesis conditions. For H-Knt, a slight increase in the S_{BET} value was observed, reaching 38 m^2/g. However, higher values of 76 m^2/g and 84 m^2/g have been reported for similar materials [20,34]. The A.P.D. decreased from 14 nm to 12 nm. In contrast, H-Knt exhibited a higher T.P.V. of 0.23 cc/g compared with Na-Knt (0.20 cc/g). This increase could be associated with the particle reorganization after acid treatment and the voids formed between the Knt particles.

Table 2. Textural properties of Na-Knt and H-Knt samples.

Sample	A.P.D (nm)	T.P.V. (cc/g)	S_{BET} (m^2/g)
Na-Knt	14	0.20	29
H-Knt	12	0.23	38

2.7. BB-41 Removal Performance

2.7.1. Effect of Initial Concentration

The initial concentration (C_i) is considered one of the important factors affecting removal properties [41]. Herein, the C_i values were varied from 25 mg/L to 1000 mg/L. When H-Knt was used, the removed amount (expressed in mg/g) increased from 23 mg/g to 56 mg/g at lower C_i values between 25 mg/L and 200 mg/L, followed by a slight increase to 61 mg/g as the C_i value increased to 1000 mg/L (Figure 3A). This increase was attributed to the higher driving force that promotes diffusion and mass transfer from the solution to the surface of the adsorbent [42–44]. However, a considerable increase in removal efficiency (expressed as percentage) was observed as the C_i value decreased. The removal efficiency increased from 38% to 85% as C_i decreased from 200 to 25 mg/L and reached 25% at 1000 mg/L (Figure 3A). In this case, more dye molecules were available than the number of removal sites on the H-Knt material.

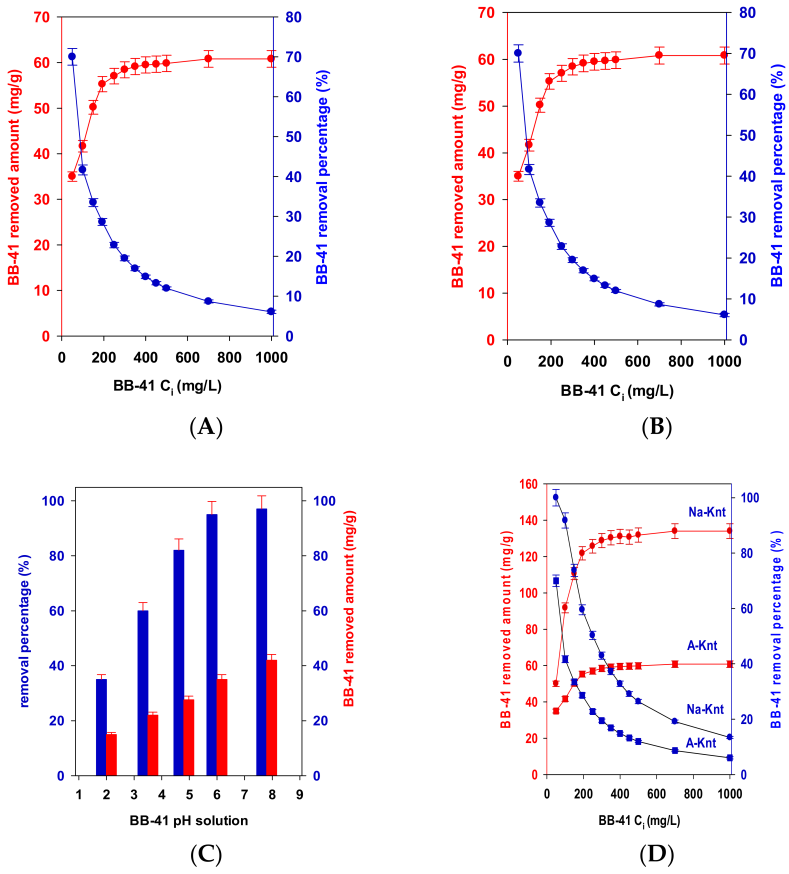


Figure 3. Effect of different parameters on the removal properties of BB-41 using H-Knt sample. (**A**) initial concentration, (**B**) used mass, (**C**) BB-41 pH solution, (**D**) acid treatment of Na-Knt. (blue lines and bar) removal percentage and (red lines and bar) removed amount.

2.7.2. Effect of Sample Dose

In the previous section, the population of removal sites was kept constant. In this section, however, it was varied by increasing the H-Knt dosage while keeping the number of dye molecules fixed (C_i = 200 mg/L). This investigation was performed to determine the optimal H-Knt dose and to avoid inefficiencies and unnecessary expenses.

As shown in Figure 3B, the removal efficiency increased continuously from 20% to 66% as the H-Knt mass increased from 0.025 g to 1.00 g. This improvement was attributed to the increase in the number of available removal sites at higher adsorbent dosages. In contrast,

the removed amount decreased with increasing H-Knt mass (Figure 3B). At the lowest dose of 0.025 g, a maximum removed amount of 160 mg/g was achieved, whereas a lower value of 13 mg/g was recorded when 1 g was used. This decrease may be attributed to particle agglomeration, which reduced the availability of active removal sites [45]. Therefore, a mass of 0.1 g provided a good compromise and was used in subsequent experiments.

2.7.3. Effect of pH

Effect of BB-41 Solution pH

The pH of the dye solution is one of the main factors to be considered in the removal process [41]. Herein, the pH values were varied from 2 to 11. As the pH increased, both the removed amount and removal percentage increased (Figure 3C). In particular, within the pH range of 4–8, the removed amount increased from 30 to 102 mg/g, while the removal efficiency improved from 15% to 51%. At pH values higher than 10, BB-41 underwent structural changes and predominantly formed a brown precipitate; and further experiments were not performed at pH values above 9. Given that BB-41 has a pK_{a1} of 10–11, it primarily exists in its cationic form below this range, allowing strong electrostatic attraction between BB-41 and the negatively charged surface of H-Knt [26]. Given that Na-Knt was treated with HCl, the suspension of H-Knt in deionized water showed a pH value close to 3.5. A comparable value was reported for a suspension of protonic magadiite in deionized water [26]. When H-Knt was added to the BB-41 solution, the final pH of the mixture was ~3, resulting in a low removed amount of BB-41. However, when BB-41 solutions with higher initial pH values were used, the final pH was not significantly affected, leading to improved removal amounts. Different behavior was observed when Na-Knt was used. The suspension of Na-Knt in deionized water had a pH of ~8.5 [14]. Therefore, adding Na-Knt to the BB-41 solution increased the final pH, which improved the removed amount of BB-41 dye (Figure S7) [15].

Effect of H-Knt Solid pH

In this part, H-Knt was treated with NaOH solution to modify its character from acidic to basic. The pH of the BB-41 solution was used without modification. When H-Knt was treated with low concentrations of NaOH solution, only a minor variation in the removed amount of BB-41 was observed. However, increasing the NaOH concentration resulted in a significant improvement in the removed amounts of BB-41. The final pH of the BB-41/H-Knt mixture was higher than that of the pure BB-41 dye solution. Similar results were obtained with H-magadiite [15]. As previously reported, pH affects both the chemistry of dyes and the surface charge of adsorbents [43,44]. The pH point of zero charge (pH_{pzc}) is defined as the pH at which the surface of a solid is electrically neutral or has equal densities of positive and negative charges. Knowing this value allows different strategies to be adopted to modify the surface charge of the solid and optimize it for the removal of specific cationic or anionic dyes. The starting Na-Knt exhibited a pH_{pzc} of 8 [15], while this value decreased to 3 for the H-Knt sample, confirming its acidic character. Similar behavior has been reported for other layered material [46]. These data indicate that at pH values higher than 3, H-Knt exhibits a negatively charged surface, thereby enhancing the removal of cationic BB-41 dyes. At pH values lower than 3, the surface of H-Knt becomes positively charged, which reduces the electrostatic attraction between BB-41 cations and the H-Knt surface.

2.7.4. Effect of HCl Reaction

The removal capacity for BB-41 was affected by the treatment of Na-Knt with HCl solution (Figure 3D). For H-Knt, the removal percentages decreased from 70% to 41% at lower C_i values, from 50 mg/L to 100 mg/L. Na-Knt exhibited different behavior; within the

C_i range of 50–200 mg/L, 100% removal was achieved. At C_i values higher than 200 mg/L, the removal efficiency of H-Knt decreased continuously and remained lower than that of Na-Knt (Figure 3D). Comparable results have been reported for acidic magadiite and acid-activated clay minerals [26,46]. As previously stated for acidic magadiite, the pH of the solid affected the reduction in removal efficiency, which may also explain the behavior of the H-Knt sample. As the positive surface charge increased under acidic conditions, the electrostatic interaction with the positively charged dye species decreased. As reported in previous studies, specific surface area can enhance the efficiency of removal agents; however, in some cases, it may not be the dominant factor.

2.7.5. Isotherm Model Fitting

Two parameters Langmuir, Freundlich models are used to assess the removal performance of BB-41 on Na-Knt and H-Knt [47]. Their applicability was evaluated by fitting the experimental data to their linearized forms (Equations (S3) and (S5)). The corresponding parameters are summarized in Table 3.

Table 3. Isotherm model parameters for the removal of BB-41.

Isotherm Model	Na-Knt	H-Knt
Langmuir		
q_{max} (mg/g)	137 (131) *	62 (61)
K_L (L/mg)	0.1137 (0.2508)	0.0544 (0.0662)
R^2	0.9997 (0.9928)	0.9996 (0.9999)
χ^2	—(1.67)	—(1.92)
Freundlich		
K_F (mg/g) $(L/mg)^{1/n}$	82 (81)	25 (23)
$1/n_F$	0.0821 (0.0821)	0.1454 (0.1624)
R^2	0.9050 (0.9904)	0.8864 (0.9999)
χ^2	—-(1.71)	—-(2.73)
Sips		
q_{max} (mg/g)	143	60
K_s $(L/mg)^{n}{}_s$	0.5972	0.0544
n_s	1.94	1.67
R^2	0.9931	0.9985
χ^2	0.152	0.914

* related to the non-linear fitting model.

The experimental data of Na-Knt and H-Knt samples showed a notable fit to the Langmuir equation, with an R^2 value of 0.9997 compared with 0.8864 for the Freundlich model under the tested conditions (Figures S8(left) and S9(left)). In contrast, the Freundlich isotherm showed a less acceptable fit, with 1/n values lower than 1 (Figures S8(right) and S9(right)). Na-Knt exhibited a K_L constant value of 0.1137 L/g, which was higher than that of H-Knt (0.0544 L/g), indicating the higher affinity of Na-Knt for BB-41 molecules.

The parameters derived from the non-linear fitting Langmuir and Freundlich models (Equations (S4) and (S6)) are presented in Table 3. The equation of chi square (χ^2) is shown Equation (S13) in the Supporting Information [48]. Based on the higher regression coefficient (R^2) and the lower Chi square (χ^2) values, the isotherm data fitted well the Langmuir model. The Na-Knt had a q_{max} value of 131 mg/g higher than of H-Knt sample of 61 mg/g. The higher K_L value confirms the higher affinity of Na-Knt to BB-41 dye. Although H-Knt exhibited a high regression coefficient of 0.9999, the lowest χ^2 value of 2.7 was achieved. Comparing the three isotherm models, the Sips model resolved this ambiguity with the highest regression coefficient and the lowest χ^2 value. The "n_s" of

H-Knt was higher compared to the Na-Knt value, and this could indicate that the acid treatment actually enhanced surface energetic homogeneity.

When Na-Knt was treated with a HCl solution, the number of Si-OH increased, and it affected the q_{max} for the H-Knt sample. The reduction was related to the decrease in the population of removal sites and/or the lower pH value of the H-Knt solid. In the case of Na-Knt, the removal sites have been reported to be easily accessible to BB-41 cations through ion-exchange reactions with Na cations [26]. In addition, Na-Knt was prepared in an alkaline environment; therefore, once added to the contaminant solution, it increased the pH of the suspension, thereby affecting the removal process [26]. A significant improvement was observed when H-Knt was soaked in NaOH solution before being added to the dye solution. Moreover, the H-Knt sample was converted to Na-Knt, as confirmed by PXRD data, with a shift in d_{001} from 1.61 nm to 1.92 nm after treatment with 1 M NaOH solution [26]. This behavior can be explained by the deprotonation of hydroxyl groups, which made the surface negatively charged and enhanced the removal properties through electrostatic attraction.

When the maximum removal capacity (q_{max}) of the H-Knt sample was compared with those of different acid-activated magadiites and aluminosilicate materials, H-Knt exhibited a value of 62 mg/g. This value was lower than that of untreated Na-Knt. Overall, the acid activation process did not improve the removal capacity of the treated samples, mainly due to the decrease in cation-exchange capacity and the reduction in available removal sites (Table 4).

Table 4. Removal efficiency of selected silicates and aluminosilicate materials.

Samples	q_{max} (mg/g)	References
Na-Knt	131 *	This study
H-Knt	61 *	This study
Brick wastes (BW)	25	[49]
Acid Activated BW	15	[49]
Saudi Local Clay (SLC) [+]	50	[50]
Acid activated SLCs	47–73	[50]
Polymer Grade Mt (PG)	81	[46]
Acid activated PGs	37–72	[46]
Na-Magadiite (Na-Mgd)	219	[26]
Protonated magadiite (H-Mgd)	114	[26]

[+] SLC; Saudi Local Clay. * reported from the non-linear Langmuir fitting.

2.7.6. Kinetic Study

The kinetic study is useful for understanding the removal mechanism involved in the process by determining the reaction order [51]. PFO and PSO linear models are employed to correlate the removal kinetic data, and the calculated parameters are summarized in Table 5. The corresponding kinetic plots are presented in the Supporting Information (Figures S11A,B and S12A,B).

The correlation coefficients (R^2) for PFO model were in the range of 0.93 to 0.96, and the predicted q_{cal} values deviated significantly from the q_{exp} one. Thus, this PFO model was not suitable to fit the experimental data. In contrast, the PSO model indicated that the correlation coefficients (R^2) were higher (0.9952 to 0.9995) and the q_{cal} values agreed closely with the q_{exp} ones. Thus, PSO model described accurately the removal behavior of BB-41 on Na-Knt and H-Knt samples.

When using a nonlinear model, the values of the error functions are also crucial; R^2 values are said to be insufficient to determine whether a certain model is appropriate. In fact, it was strongly advised to use the nonlinear approach to accurately estimate the parameters

of kinetic models [52]. The parameters of the PFO and PSO non-linear tests are summarized in Table 5.

Table 5. Parameters of the different kinetic models for BB-41 removal on Na-Knt and H-Knt samples.

Model	Parameters	Na-Knt	H-Knt
PFO	q_{exp} (mg/g)	122	55
	q_{cal} (mg/g)	92 (114) *	35 (50)
	k_1 (1/h)	0.2233 (0.4559)	0.3201 (1.062)
	R^2	0.9679 (0.9943)	0.9306 (0.9943)
	SSE%	12	7.34
PSO	q_{exp} (mg/g)	122	55
	q_{cal} (mg/g)	127 (125)	57 (54)
	k_2 (g/(mg.h))	0.00418(0.005566)	0.03358 (0.0222)
	R^2	0.9995 (0.9952)	0.9955 (0.9982)
	SSE%	8.77	5.32
Film diffusion	$k_{i,1}$ (mg/(g.$h^{0.5}$))	30.08	13.51)
	C_1	20.58	16.39
	R_1^2	0.9978	0.9917
Intraparticle diffusion	$k_{i,2}$ (mg/(g.$h^{0.5}$))	2.96	0.6515
	C_2	107	51.96
	R_2^2	0.9643	0.9171

q_{exp}: q experimental. q_{cal}: q calculated from the model. * values deduced from the non-linear fitting model.

The R^2 values were improved for both models, and lower SSE % values were obtained for the PSO model, confirming the suitability of PSO model to fit the experimental data. Although an improvement of R^2 (about 0.9943 and 0.9982) and lower values for SSE % were obtained for PFO model, the q_{cal} values were lower than the q_{exp} ones, implying the non-suitability of this model to fit the experimental data.

For the intra particle (ID) model, the non-linear test was employed; the data are presented in Figure 4. If the plot of q_{exp} versus $t^{1/2}$ gives a straight line that passes through the origin, it means that intraparticle diffusion is the sole rate-controlling mechanism; however, a non-zero intercept means that additional mechanisms are involved in the adsorption [53]. However, the Na-Knt and H-Knt samples exhibited two linear steps. The first step was attributed to the film diffusion (also known as external diffusion) of BB-41 cations in the solution to the external surfaces of Na-Knt and H-Knt. The second one is associated with the intraparticle diffusion stage resulted to the diffusion of the BB-41 cations from the exterior surface into the interlayer spacing. The Na-Knt sample exhibited a higher $k_{i,1}$ value than the H-Knt one, reflecting the faster film diffusion and easy intercalation of BB-41 cations into the interlayer spacing of Na-Knt compared to the H-Knt sample. The $k_{i,2}$ values for both samples were lower than the $k_{i,1}$ ones, indicating slower intraparticle diffusion process with high extend for H-Knt. The intercept of the second step usually gives insight into the thickness of the boundary layer involved in the removal process [54]. This thickness was higher for Na-Knt. These data indicated that external mass transfer and intra particle diffusion worked together to control the overall removal process [55].

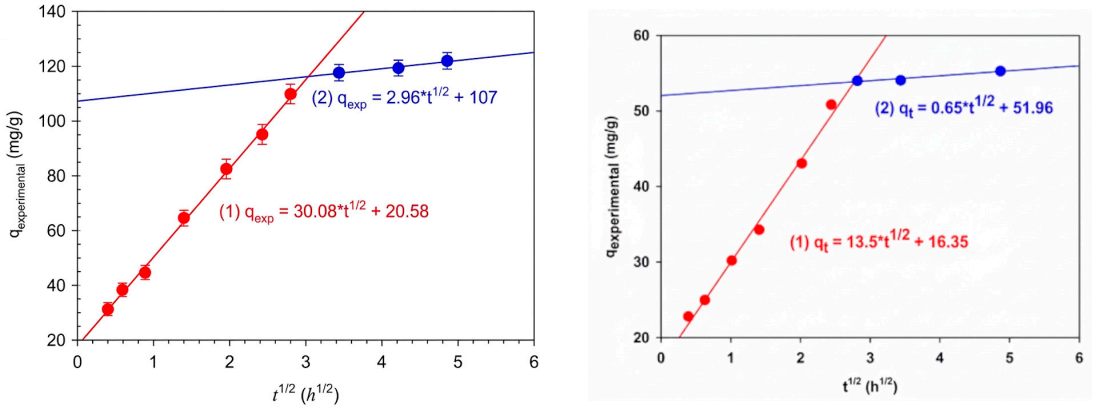


Figure 4. Intraparticle diffusion plot of BB-41 removal on (**left**) Na-Knt and (**right**) H-Knt samples.

2.7.7. Regeneration Tests Data

Regeneration is considered an important factor in the removal process, as it reduces the mass of spent adsorbent and helps avoid potential pollution caused by adsorbent disposal [56]. In the present study, regeneration tests were carried out using a C_i of 200 mg/L. During the first four regeneration cycles, Na-Knt retained 82% of its original removal efficiency and then progressively decreased to 67% as the number of cycles increased. After the seventh cycle, a further decrease of 40% was observed (Figure 5A). In contrast, the H-Knt sample exhibited different behavior. The regeneration results showed that the tested material retained its initial removal efficiency to 83% after four cycles, with slight variation of 4%. This value was retained with an average of 75% of initial value even after 7th cycle (Figure 5A). The variation in the BB-41 amount removed after each regeneration cycle is presented in Figure 5B. Generally speaking, the initial removed amount of 29.8 mg/g was retained after the second cycle, of up to 28.00 mg/g; then, it decreased gradually to 17.80 mg/g after the seventh cycle. On the other hand, the removed amount by H-Knt kept changing slightly after the seventh cycle, with a variation from 14.30 mg/g to11.00 mg/g.

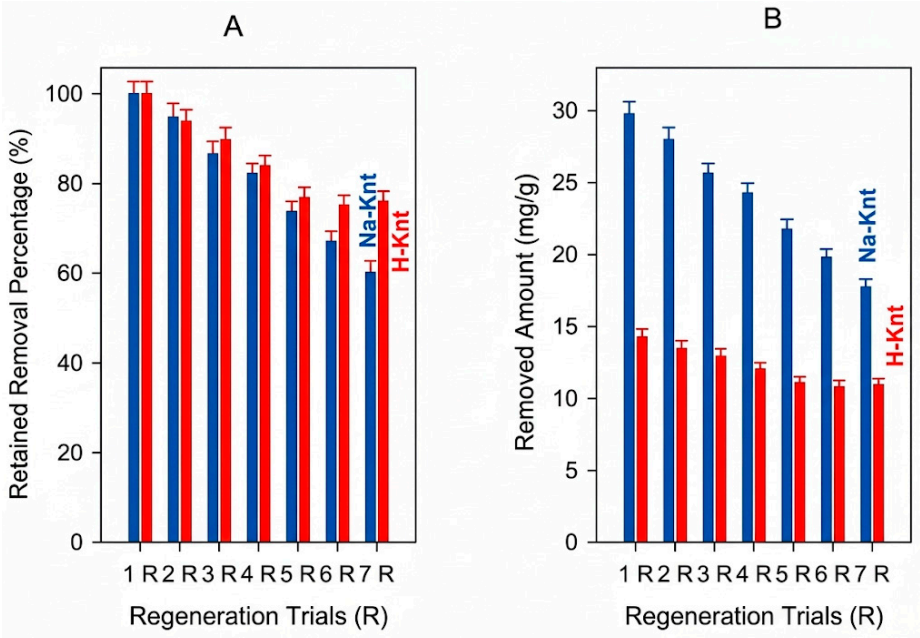


Figure 5. Regeneration tests of Na-Knt (blue bars) and H-Knt (red bars) samples. (**A**) Retained removal percentage (%) and (**B**) retained removed amount.

The data indicated that H-Knt retained a higher percentage, and it did not demonstrate an easier oxidative degradation. We hypothesize that the altered surface acidity and textural properties of H-Knt may influence the accessibility of sulfate radicals generated via oxone activation to the adsorbed dye molecules [26]. The complete mineralization of BB-41 dye cations could not be confirmed, since Total Organic Content (TOC) and Chemical Oxygen Demand (COD) measurements were not performed and were outside the scope of this study. Additionally, there is a concern about potential secondary contamination from trace cobalt (Co^{2+}) leaching in water, which has not been quantified yet and represents a significant limitation that needs to be addressed in future investigation.

2.7.8. Empirical Single-Batch Design Procedure

This procedure allows one to estimate theoretically the required masses to remove a certain amount of dye. Thus, it helps in controlling costs and reduces the production of contaminated sludge [57]. This design is based on the mass balance equation and the parameters of the isotherm models [58].

Equation (1) presents the mass balance relationship between the input and the output concentrations during the removal process, as follows:

$$\frac{M}{V} = \frac{C_o - C_e}{q_e} \quad (1)$$

By substituting the expression of q_e from the Langmuir model into Equation (1), a new formula is obtained, as shown in Equation (2).

$$\frac{M}{V} = \frac{C_o - C_e}{\frac{q_{max} K_L C_e}{1 + K_L C_e}} \quad (2)$$

Equation (2) was modified to Equation (3) using the initial concentration (C_o) and desired removal percentage (R%).

$$\frac{M}{V} = \frac{\left(\frac{R\%}{100}\right) C_o}{\frac{q_{max} K_L \left(1 - \frac{R\%}{100}\right) C_o}{1 + K_L \left(1 - \frac{R\%}{100}\right) C_o}} \quad (3)$$

Meanwhile, Equation (4) represents the M/V relationship based on the Freundlich model.

$$\frac{M}{V} = \frac{\left(\frac{R\%}{100}\right) C_o}{K_F \left(\left(1 - \frac{R\%}{100}\right) C_o\right)^{1/n}} \quad (4)$$

Figure 6 shows the relationship between the required masses for specific removal percentages and the treated effluent volumes. Two general trends were observed. First, as the treated volume increased, higher masses were required to achieve a fixed removal percentage. Second, as the targeted removal percentage increased, higher masses were also required for a fixed treated effluent volume.

The required masses of H-Knt were 22.59 g, 29.31 g, 37.82 g, 49.80 g, 71.38 g, and 96.00 g to treat 10 L of effluent at a fixed initial concentration of 200 mg/L and removal percentages of 50%, 60%, 70%, 80%, 90%, and 95%, respectively (Figure 6B). These values were lower when Na-Knt was tested, where 8.00 g, 9.79 g, 11.80 g, 14.35 g, 19.05 g, and 26.26 g were required under the same removal conditions (Figure 6A). The difference between the two samples was related to their maximum removal capacities (q_{max}). H-Knt exhibited a q_{max} value of 62.35 mg/g, which was lower than that of Na-Knt (136.6 mg/g). Comparable results have been obtained for different materials with different removal capacity values [15,26].

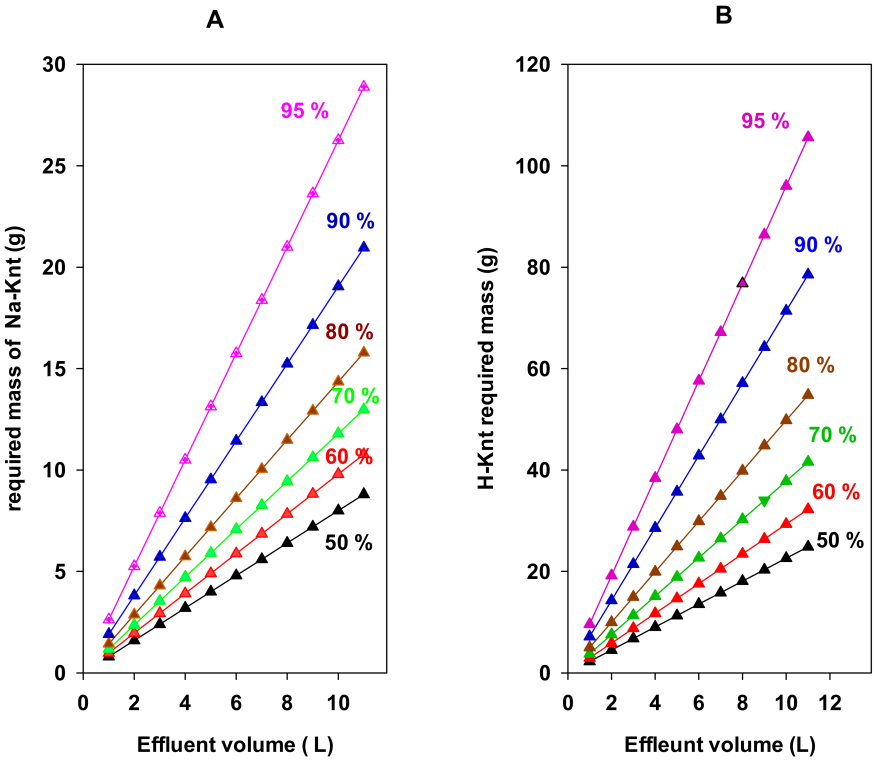


Figure 6. Estimation of required masses of (**A**) Na-Knt and (**B**) H-Knt to treat different effluent volumes of BB-41 at different removal percentages and fixed initial concentration of 200 mg/L.

It has been reported that the selected isotherm model affects the calculated mass at higher removal percentages between 80% to 95%. In some cases, the Langmuir model overestimates the required masses compared to the Freundlich model, whereas in other cases, the Freundlich model overestimated these values. Therefore, the choice of isotherm model should be made carefully during the design process [59]. In the present study, the Freundlich model was also used for the design. For both samples, the Freundlich model underestimated the required masses at removal percentages of 50%, 60%, 70%, 80%, 90%, and 95%, as shown in Figures S13 and S14. For example, to treat 10 L of effluent with a targeted removal percentage of 95%, the calculation indicated that 86.49 g of H-Knt was required. This value was lower than that obtained from the Langmuir model, of 96.00 g [26].

To overcome this limitation, the use of the Sips model was proposed [59]. This model is considered a hybrid, or combination, of both Langmuir and Freundlich models. Using the parameters model (Table 2), the M/V ratio was expressed as shown in Equation (5).

$$\frac{M}{V} = \frac{C_o - C_e}{\frac{q_{max} K_S (C_e)^{n_s}}{1 + K_S (C_e)^{n_s}}} \quad (5)$$

Figure 7 compares the masses of Na-Knt (left) and H-Knt (right) required to treat different effluent volumes, with a C_i of 200 mg/L, at a fixed removal percentage of 95% using Langmuir and Sips models. The Sips model underestimated the required masses of Na-Knt and H-Knt by 23% and 32% targeting a removal percentage of 95%, respectively. Similar observations were reported when a biosorbent was investigated [59]. This difference was attributed to the shape of the isotherms at lower concentrations [59], and confirmed that the choice of isotherm model is crucial step during the design process.

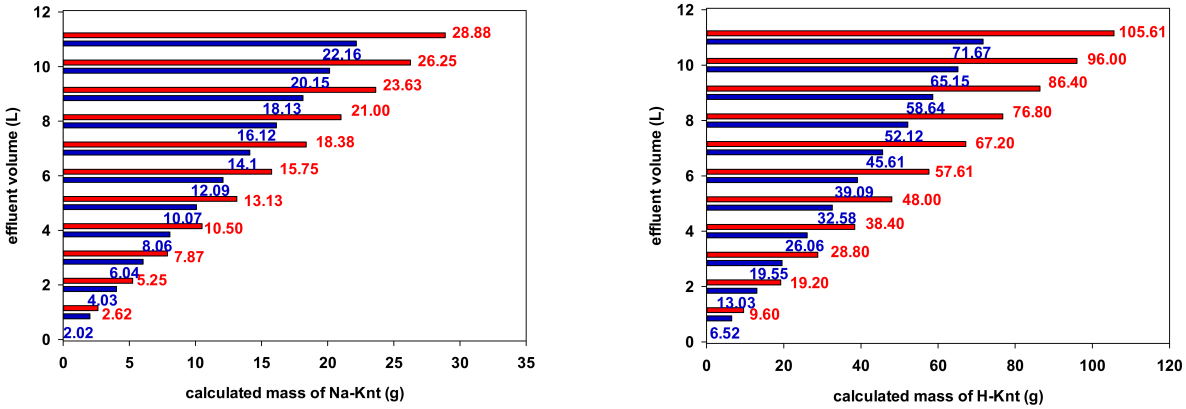


Figure 7. Estimation of required masses of (**left**) Na-Knt and (**right**) H-Knt to treat different effluent volumes of BB-41 at a fixed removal percentage of 95% using Langmuir (red bars) and Sips (blue bars) models.

By varying the initial effluent concentrations while fixing the removal percentage at 95% and the volume at 10 L, calculations using the Sips model indicated that the required masses of both Na-Knt and H-Knt increased as C_i increased. As shown in Figure 8, the calculated masses of Na-Knt were lower an average about 65%) than those of H-Knt. This difference was attributed to the maximum removed capacities (q_{max}) of the two samples [15,26]. Additional experimental validation at larger volumes or under realistic wastewater conditions are needed. The influence of salts, competing ions, other dyes, and dissolved organic matter should be taken into account.

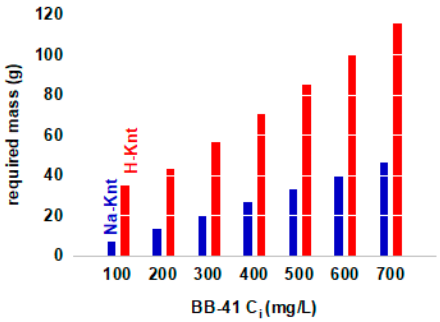


Figure 8. Required masses of Na-knt (blue bars) and H-Knt (red bars) to treat a fixed volume of 10 L using different BB-41 initial concentrations (mg/L) at a removal percentage of 95% and using non-linear Sips model.

3. Experimental Part

All chemicals used in this study were of reagent grade with a purity higher than 95%. The silica source (fumed silica) as well as sodium hydroxide (NaOH), hydrochloric acid (HCl), and BB-41 ($C_{20}H_{26}N_4O_6S_2$) dye were obtained from Aldrich (St. Louis, MO, USA). Oxone ($2KHSO_5{\cdot}KHSO_4{\cdot}K_2SO_4$) and cobalt nitrate ($Co(NO_3)_2{\cdot}6H_2O$) salt were supplied by Acros Organics (Loughborough, UK). All chemicals were used without further purification. Deionized water was used for the preparation of precursors and solutions.

3.1. Synthesis of Na-Kenyaite and H-Kenyaite

Na-kenyaite (Na-Knt) is rarely found in nature, and it was prepared as follows [15]: 105 mL of NaOH solution (1.14 M) and 16 g of solid fumed silica were stirred for 30 min at room temperature and then transferred to a Teflon-lined autoclave. The autoclave was placed in an electric oven at 170 °C for 2 days. Afterward, the autoclave was rapidly immersed

in an ice bath for cooling. The sample was then filtered, rinsed with deionized water, and air-dried at room temperature for overnight.

To obtain the protonic kenyaite (H-Knt) sample, 1 g of Na-Knt was dispersed into 25 mL of HCl solution (0.1 M) and mixed for 3 h at room temperature. The product was recovered by filtration, washed with water until free of Cl^- ions based on the test silver nitrate, and then dried at room temperature.

3.2. BB-41 Removal Experiments

The efficiencies of Na-Knt and H-Knt for BB-41 removal were investigated using a batch process. All experimental trials were performed in duplicates with experimental error within 3–5%. Firstly, a stock solution of 1000 mg/L was prepared by dissolving 1 g of BB-41 in 1 L of deionized water. The desired concentrations were prepared using the dilution equation. For each isotherm point, 100 mg of Na-Knt or H-Knt was added to 100 mL of BB-41 solution. The sealed tubes were shaken in a temperature-controlled water bath at 120 rpm and 25 °C for 18 h. This period was enough to ensure a complete equilibrium, as presented in Figure S10. After 18 h, the solid samples were separated by centrifugation. The supernatants were analyzed using a UV spectrophotometer (Varian, Victoria, Australia) at a maximum wavelength of 610 nm. Equations (S1) and (S2) were used to determine the removed amount (mg/g) and removal percentage (%), respectively. The experimental data were fitted using Linear and non-linear Langmuir (Equations (S3) and (S4)), Freundlich (Equations (S5) and (S6)), and Sips (Equation (S7)) models, as reported in the Supporting Information.

3.3. Kinetic Studies

The removal kinetics were conducted at an initial BB-41 concentration of 200 mg/L. A total of 0.100 g of solid adsorbent was added to 100 mL of BB-41 solution in a conical flask. The flask was shaken at 120 rpm and 25 °C in water bath. A total of ten individual 0.1 mL aliquots at predetermined time intervals were withdrawn using small syringe filters. The total withdrawn volume of 1 mL represented less than 1% of the solution volume, the adjustment for volume variation had a negligible effect on concentration changes and on removed amounts (q_t). After dilution, the BB-41 concentrations were measured using an UV-spectrophotometer. The experimental data were fitted using linear and non-linear pseudo-first-order (PFO, Equations (S8) and (S9)), pseudo-second-order (PSO, Equations (S10) and (S11)), and intra particle diffusion kinetic (Equation (S12)) models to elucidate the removal mechanism. The equations are presented in the Supporting Information.

3.4. Regeneration Tests Procedure

The regeneration tests were performed using a sulfate radical-based oxidation method. Amounts of 0.2 g of Na-Knt or H-Knt samples were added to 50 mL of BB-41 solution (with concentration of 200 mg/L) for 6 h at room temperature. After solid separation, the spent materials were mixed with a 10 mL of $Co(NO_3)_2{\cdot}6H_2O$ aqueous solution (9.74 mM). The Co^{2+} cations were served as the homogeneous catalyst. Then, 8 mg of the oxidant oxone ($2KHSO_5 \times KHSO_4 \times K_2SO_4$) was added to the mixture to degrade the removed BB-41 for 30 min at room temperature. After centrifugation, the separated solids were rinsed five or six times with deionized water before being reused in the subsequent run following the reported procedure above. For each run, the supernatant was analyzed and removal percentage was calculated. All experimental trials were performed in duplicates with experimental error within 3–5%.

3.5. Characterization Methods

An Advance 8 X-ray diffractometer (Bruker AXS, Karlsruhe, Germany) with Cu Kα radiation was used to analyze the structure of the prepared samples. XRF model S4 EXPLORER (Bruker AXS, Karlsruhe, Germany) was utilized to obtain the chemical composition. FTIR spectra were obtained using the KBr disc method with a Bio-Rad spectrometer (Hercules, CA, USA). Micrographs of the Na-Knt and H-Knt samples were obtained by SEM using a JEOL JSM-6700F instrument equipped with EDX system (Tokyo, Japan). The thermal characteristics of the Na-Knt and H-Knt samples were investigated using a thermogravimetric analyzer, model SDT2960 (TA Instrument New Castle, DE, USA). ^{29}Si MAS NMR spectra were collected using a Bruker AX 400 spectrometer (Bruker, Karlsruhe, Germany) The run details were reported elsewhere [26]. Nitrogen adsorption isotherms were measured using a Quantachrome S6 autosampler (Quantachrome, Boynton Beach, FL, USA) to determine the specific surface area (S_{BET}), total pore volume (T.P.V.), and average pore diameter (A.P.D.). The samples were outgassed overnight at 120 °C before analysis. The point of zero charge (pH_{pzc}) was determined using pH-drift method. The concentration of BB-41 in the supernatants after equilibrium was measured using a Cary 100 spectrophotometer (Varian, Victoria, Australia) using an established calibration curve.

Supplementary Materials: The following supporting information can be downloaded at: https://www.mdpi.com/article/10.3390/inorganics14110291/s1, Figure S1: Deconvolution of ^{29}Si MAS NMR of Na-kenyaite (Na-Knt) sample; Figure S2: Deconvolution of ^{29}Si MAS NMR of H-kenyaite (H-Knt) sample. Figure S3. Deconvolution of FTIR spectrum in the hydroxyl region for Na-Knt sample. Figure S4. Deconvolution of FTIR spectrum in the Si-O-Si region for Na-Knt sample. Figure S5. Deconvolution of FTIR spectrum in the hydroxyl region for H-Knt sample. Figure S6. Deconvolution of FTIR spectrum in the Si-O-Si region for H-Knt sample. Figure S7. Effect of BB-41 solution pH on the removal properties of Na-Knt sample: (grey bars) removal percentage (R %) and (red bars) removed amount (q_e). Figure S8. Langmuir (red line) and Freundlich (blue line) linear fittings of the experimental data related to Na-Knt sample. Figure S9. Langmuir (red line) and Freundlich (blue line) linear fittings of the experimental data related to H-Knt sample. Figure S10. Effect of contact time (h) on the removal of BB-41 dye using Na-Knt (red color) and H-Knt (blue color) samples. Figure S11. Linear fitting of (A) the pseudo-first-order (PFO) and (B) pseudo-second-order (PSO) models, respectively for Na-Knt sample. Figure S12. Linear fitting of (A) the pseudo-first-order (PFO) and (B) pseudo-second-order (PSO) models, respectively for H-Knt sample. Figure S13. Comparison between Langmuir and Freundlich models for the estimated masses calculation using Na-Knt. Figure S14. Comparison between Langmuir and Freundlich models for the estimated masses calculation using H-Knt.

Author Contributions: Conceptualization, R.A.-F., S.A.P., S.R. and F.K.; Methodology, M.G.A., T.S.A., S.A.P., S.R., H.O.H., A.O.L. and F.K.; Software, S.A.P., H.O.H. and A.O.L.; Validation, R.A.-F., M.G.A., T.S.A. and A.O.L.; Formal analysis, R.A.-F., T.S.A. and H.O.H.; Investigation, R.A.-F., M.G.A., S.A.P. and S.R.; Resources, S.A.P. and F.K.; Data curation, M.G.A., T.S.A. and F.K.; Writing—original draft, R.A.-F., M.G.A., T.S.A., S.A.P., S.R., H.O.H., A.O.L. and F.K.; Writing—review & editing, S.A.P., S.R., A.O.L. and F.K.; Visualization, H.O.H.; Supervision, F.K.; Project administration, F.K. All authors have read and agreed to the published version of the manuscript.

Funding: This research received no external funding.

Institutional Review Board Statement: Not applicable.

Informed Consent Statement: Not applicable.

Data Availability Statement: The original contributions presented in this study are included in the article/Supplementary Material. Further inquiries can be directed to the corresponding authors.

Conflicts of Interest: The authors declare no conflicts of interest.

References

1. Kathing, C.; Saini, G. A review of various treatment methods for the removal of dyes from textile effluent. *Recent Prog. Mater.* **2022**, *4*, 1–15. [CrossRef]
2. Crini, G.; Lichtfouse, E. Advantages and disadvantages of techniques used for wastewater treatment. *Environ. Chem. Lett.* **2019**, *17*, 145–155. [CrossRef]
3. Hynes, N.R.J.; Kumar, J.S.; Kamyab, H.; Sujana, J.A.J.; Al-Khashman, O.A.; Kuslu, Y.; Ene, A.; Kumar, B.S. Modern enabling techniques and adsorbents based dye removal with sustainability concerns in textile industrial sector—A comprehensive review. *J. Clean. Prod.* **2020**, *272*, 122636. [CrossRef]
4. Kumar, P.S.; Joshiba, G.J.; Femina, C.C.; Varshini, P.; Priyadharshini, S.; Karthick, M.A.; Jothirani, R. A critical review on recent developments in the low-cost adsorption of dyes from wastewater. *Desalin. Water Treat.* **2019**, *172*, 395–416. [CrossRef]
5. Pérez-Botella, E.; Valencia, S.; Rey, F. Zeolites in adsorption processes: State of the art and future prospects. *Chem. Rev.* **2022**, *122*, 17647–17695. [CrossRef]
6. Phuekphong, A.; Imwiset, K.; Ogawa, M. Designing nanoarchitecture for environmental remediation based on the clay minerals as building block. *J. Hazard. Mater.* **2020**, *399*, 122888. [CrossRef]
7. Leal, P.V.B.; Magriotis, Z.M.; de Sales, P.F.; Papini, R.M.; Viana, P.R.D.M. Effect of the acid treatment conditions of kaolinite on etheramine adsorption: A comparative analysis using chemometric tools. *J. Environ. Manag.* **2017**, *197*, 393–403. [CrossRef]
8. Hassan, M.; Naidu, R.; Du, J.; Liu, Y.; Qi, F. Critical review of magnetic biosorbents: Their preparation, application, and regeneration for wastewater treatment. *Sci. Total Environ.* **2020**, *702*, 134893. [CrossRef]
9. Liu, Y.; Biswas, B.; Hassan, M.; Naidu, R. Green adsorbents for environmental remediation: Synthesis methods, ecotoxicity, and reusability prospects. *Processes* **2024**, *12*, 1195. [CrossRef]
10. Biswas, B.; Warr, L.N.; Hilder, E.F.; Goswami, N.; Rahman, M.M.; Churchman, J.G.; Vasilev, K.; Pan, G.; Naidu, R. Biocompatible functionalisation of nanoclays for improved environmental remediation. *Chem. Soc. Rev.* **2019**, *48*, 3740–3770. [CrossRef]
11. Kausar, A.; Iqbal, M.; Javed, A.; Aftab, K.; Nazli, Z.; Nawaz, H.; Bhatti, H.N.; Nouren, S. Dyes adsorption using clay and modified clay: A review. *J. Mol. Liq.* **2018**, *256*, 395–407. [CrossRef]
12. Ewis, D.; Ba-Abbad, M.M.; Benamor, A.; El-Naas, M.H. Adsorption of organic water pollutants by clays and clay minerals composites: A comprehensive review. *Appl. Clay Sci.* **2022**, *229*, 106686. [CrossRef]
13. Lim, W.T.; Jang, J.H.; Park, N.Y.; Paek, S.M.; Kim, W.C.; Park, M. Spontaneous nanoparticle formation coupled with selective adsorption in magadiite. *J. Mater. Chem. A* **2017**, *5*, 4144–4149. [CrossRef]
14. Sirinakorn, T.; Imwiset, K.; Bureekaew, S.; Ogawa, M. Inorganic modification of layered silicates toward functional inorganic-inorganic hybrids. *Appl. Clay Sci.* **2018**, *153*, 187–197. [CrossRef]
15. Al-Madanat, O.Y.; Popoola, S.A.; Al Dmour, H.; Al-Faze, R.; Kooli, F. Na-Kenyaite as efficient basic blue-41 dye removal: Synthesis and regeneration studies. *Water* **2024**, *16*, 2056. [CrossRef]
16. Aicha, B.; Mohamed, S.; Jocelyne, M.-B.; Benedicte, L.; Jean-Luc, B.; Abdelkader, B. Preparation of new microporous titanium pillared kenyaite materials active for the photodegradation of methyl orange. *J. Porous Mater.* **2017**, *25*, 801–812. [CrossRef]
17. Kalvachev, Y.; Kostov-Kytin, V.; Todorova, S.; Tenchev, K.; Kadinov, G. Synthetic kenyaite as catalyst support for hydrocarbon combustion. *Appl. Catal. B Environ.* **2006**, *66*, 192–197. [CrossRef]
18. Park, K.-W.; Joo, E.-R.; Kwon, O.-Y. Synthesis of SiC from kenyaite-carbon nanocomposite using cobalt catalyst. *Appl. Clay Sci.* **2019**, *183*, 105317. [CrossRef]
19. Feng, Z.; Wang, Y.; Lv, T.; Zhang, S.; Liu, X.; Liu, X.; Meng, C. Hydrothermal conversion of kenyaite into zeolite omega in tetramethylammonium cations system. *Solid State Sci.* **2020**, *103*, 106196. [CrossRef]
20. Fatima, H.; Seo, J.-D.; Kim, J.; Park, M. Adsorption behavior of kenyaite for Cu^{2+} and Pb^{2+}. *J. Porous Mater.* **2021**, *29*, 111–117. [CrossRef]
21. Guerra, D.L.; Airoldi, C.; Viana, R.R. Adsorption of arsenic(V) into modified lamellar Kenyaite. *J. Hazard. Mater.* **2009**, *163*, 1391–1396. [CrossRef]
22. Royer, B.; Cardoso, N.F.; Lima, E.C.; Ruiz, V.S.; Macedo, T.R.; Airoldi, C. Organofunctionalized kenyaite for dye removal from aqueous solution. *J. Colloid Interface Sci.* **2009**, *336*, 398–405. [CrossRef]
23. Kooli, F.; Liu, Y.; Hbaieb, K.; Ching, O.; Al-Faze, R. Characterization of organo-kenyaites: Thermal stability and their effects on eosin removal characteristics. *Clay Miner.* **2018**, *53*, 91–104. [CrossRef]
24. Fernandes, J.V.A.M.; Rodrigues, A.M.; Menezes, R.R.; Neves, G.D.A. Adsorption of anionic dye on the acid-functionalized bentonite. *Materials* **2020**, *13*, 3600. [CrossRef]
25. Kwon, O.Y.; Choi, S.W. Silica-pillared H-kenyaites: Interlamellar base catalyzed-reaction of tetraethylorthosilicate in water suspension. *Bull. Korean Chem. Soc.* **1999**, *20*, 69–75. [CrossRef]
26. Alraddadi, T.S.; Alam, M.G.; Al-Faze, R.; Popoola, S.A.; Rakass, S.; Hassani, H.O.; Kooli, F. Comparative removal properties of sodium magadiite and its protonic form on Basic-Blue 41 from contaminated aqueous solution. *Inorganics* **2025**, *13*, 303. [CrossRef]

27. Royer, B.; Cardoso, N.F.; Lima, E.C.; Macedo, T.R.; Airoldi, C. Sodic and acidic crystalline lamellar magadiite adsorbents for the removal of Methylene Blue from aqueous solutions: Kinetic and equilibrium studies. *Sep. Sci. Technol.* **2009**, *45*, 129–141. [CrossRef]
28. Amari, A.; Gannouni, H.; Khan, M.I.; Almesfer, M.K.; Elkhaleefa, A.M.; Gannouni, A. Effect of structure and chemical activation on the adsorption properties of green clay minerals for the removal of cationic dye. *Appl. Sci.* **2018**, *8*, 2302. [CrossRef]
29. Liu, Y.; Yan, A.; Ding, L.; Wei, J.; Liu, Y.; Niu, Y.; Qu, R. Simultaneous and ultrafast removal of anionic and cationic dyes from aqueous solution by Zr-based MOFs hybridized by attapulgite and adsorption performance research. *Colloids Surf. A Physicochem. Eng. Asp.* **2023**, *680*, 132643. [CrossRef]
30. Kebir, Z.A.M.; Adel, M.; Adjdir, M.; Bengueddach, A.; Sassi, M. Preparation and antibacterial activity of silver nanoparticles intercalated kenyaite materials. *Mater. Res. Express* **2018**, *5*, 085021. [CrossRef]
31. Oliveira, M.E.; Filho, E.C.D.S.; Filho, J.M.; Ferreira, S.S.; Oliveira, A.C.; Campos, A.F. Catalytic performance of kenyaite and magadiite lamellar silicates for the production of α,β-unsaturated esters. *Chem. Eng. J.* **2015**, *263*, 257–267. [CrossRef]
32. Ariyapala, K.D.S.D.; Withanage, W.I.U.; Takimoto, K.; Kumada, N.; Takei, T.; Saito, N.; Horikoshi, H. Ion-exchange and antibacterial properties of layered silicate, Na-kenyaite, prepared using amorphous silicon dioxide (a-SiO_2) blocks. *J. Ceram. Soc. Jpn.* **2024**, *132*, 39–44. [CrossRef]
33. Landis, M.E.; Aufdembrink, B.A.; Chu, P.; Johnson, I.D.; Kirker, G.W.; Rubin, M.K. Preparation of molecular sieves from dense, layered metal oxides. *J. Am. Chem. Soc.* **1991**, *113*, 3189–3190. [CrossRef]
34. Park, K.-W.; Jeong, S.-Y.; Kwon, O.-Y. Interlamellar silylation of H-kenyaite with 3-aminopropyltriethoxysilane. *Appl. Clay Sci.* **2004**, *27*, 21–27. [CrossRef]
35. Park, K.-W.; Jung, J.H.; Seo, H.-J.; Kwon, O.-Y. Mesoporous silica-pillared kenyaite and magadiite as catalytic support for partial oxidation of methane. *Microporous Mesoporous Mater.* **2009**, *121*, 219–225. [CrossRef]
36. Marler, B.; Grosskreuz, I.; Gies, H. The crystal structure of synthetic kenyaite, $Na_2Si_{20}O_{40}(OH)_2{\cdot}8H_2O$. *J. Solid State Chem.* **2021**, *300*, 122215. [CrossRef]
37. Almond, G.G.; Harris, R.K.; Franklin, K.R. A structural consideration of kanemite, octosilicate, magadiite and kenyaite. *J. Mater. Chem.* **1997**, *7*, 681–687. [CrossRef]
38. Huang, Y.; Jiang, Z.; Schwieger, W. Vibrational spectroscopic studies of layered silicates. *Chem. Mater.* **1999**, *11*, 1210–1217. [CrossRef]
39. Yang, J.; Zhu, J.; Zhang, S.; Lv, T.; Feng, Z.; Wang, Y.; Meng, C. OSDA-free hydrothermal conversion of kenyaite into zeolite beta in the presence of seed crystals. *Solid State Sci.* **2020**, *107*, 106370. [CrossRef]
40. Ruiz, V.S.O.; Petrucelli, G.C.; Airoldi, C. Inorganic–organic hybrids derived from lamellar acidic kenyaite immobilizations for cation removal at the solid/liquid interface. *J. Mater. Chem.* **2006**, *16*, 2338–2346. [CrossRef]
41. Rápó, E.; Tonk, S. Factors affecting synthetic dye adsorption; desorption studies: A review of results from the last five years (2017–2021). *Molecules* **2021**, *26*, 5419. [CrossRef]
42. Mersin, G.; Açıkel, Ü.; Levent, M. Efficient adsorption of Basic Blue 41 from textile wastewaters by natural and magnetically modified Manisa-Gördes clinoptilolite. *Chem. Eng. Process.-Process Intensif.* **2021**, *169*, 108632. [CrossRef]
43. Abdu, M.; Babaee, S.; Worku, A.; Msagati, T.A.M.; Nure, J.F. The development of Giant reed biochar for adsorption of Basic Blue 41 and Eriochrome Black T azo dyes from wastewater. *Sci. Rep.* **2024**, *14*, 18320. [CrossRef]
44. Kanwal, A.; Bhatti, H.N.; Iqbal, M.; Noreen, S. Basic dye adsorption onto clay/$MnFe_2O_4$ composite: A mechanistic study. *Water Environ. Res.* **2017**, *89*, 301–311. [CrossRef]
45. He, H.; Chai, K.; Wu, T.; Qiu, Z.; Wang, S.; Hong, J. Adsorption of rhodamine B from simulated waste water onto kaolin-bentonite composites. *Materials* **2022**, *15*, 4058. [CrossRef]
46. Alraddadi, T.S.; Al-Faze, R.; Popoola, S.A.; Alam, M.G.; Rakass, S.; Al Dmour, H.; Kooli, F. Combination of acid and base activation of montmorillonite clay and its impact on the basic blue-41 removal properties: Regeneration and single batch design. *Inorganics* **2025**, *13*, 228. [CrossRef]
47. Ahmed, H.R.; Kayani, K.F.; Ealias, A.M.; Aziz, K.H.H. A comprehensive review of forty adsorption isotherm models: An in-depth analysis of ten statistical error measures. *Water Air Soil Pollut.* **2025**, *236*, 346. [CrossRef]
48. Lach, J. Analysis of the differences resulting from the determination of Langmuir isotherm coefficients from linear and non-linear forms—A case study. *Materials* **2025**, *18*, 3506. [CrossRef]
49. Kooli, F.; Yan, L.; Al-Faze, R.; Al-Sehimi, A. Removal enhancement of basic blue 41 by brick waste from an aqueous solution. *Arab. J. Chem.* **2015**, *8*, 333–342. [CrossRef]
50. Kooli, F.; Liu, Y.; Al-Faze, R.; Al Suhaimi, A. Effect of acid activation of Saudi local clay mineral on removal properties of basic blue 41 from an aqueous solution. *Appl. Clay Sci.* **2015**, *116*, 23–30. [CrossRef]
51. Kuyucu, A.E.; Selçuk, A.; Önal, Y.; Alacabey, I.; Erol, K. Effective removal of dyes from aqueous systems by waste-derived carbon adsorbent: Physicochemical characterization and adsorption studies. *Sci. Rep.* **2025**, *15*, 28835. [CrossRef]

52. Wang, J.; Guo, X. Adsorption kinetic models: Physical meanings, applications, and solving methods. *J. Hazard. Mater.* **2020**, *390*, 122156. [CrossRef]
53. Tsibranska, T.; Hristova, E. Comparison of different kinetic models for adsorption of heavy metals onto activated carbon from apricot stones. *Bulg. Chem. Commun.* **2011**, *43*, 370–377.
54. Azizian, S. Kinetic models of sorption: A theoretical analysis. *J. Colloid Interface Sci.* **2004**, *276*, 47–52. [CrossRef]
55. Saavedra-Labastida, E.; Díaz-Nava, M.C.; Illescas, J.; Muro, C. Comparison of the removal of an anionic dye from aqueous solutions by adsorption with organically modified clays and their composites. *Water Air Soil Pollut.* **2019**, *230*, 88. [CrossRef]
56. Fouda-Mbanga, B.G.; Onotu, O.; Tywabi-Ngeva, Z. Advantages of the reuse of spent adsorbents and potential applications in environmental remediation: A review. *Green Anal. Chem.* **2024**, *11*, 100156. [CrossRef]
57. Shirazi, E.K.; Metzger, J.W.; Fischer, K.; Hassani, A.H. Design and cost analysis of batch adsorber systems for removal of dyes from contaminated groundwater using natural low-cost adsorbents. *Int. J. Ind. Chem.* **2020**, *11*, 101–110. [CrossRef]
58. Debnath, S.; Ballav, N.; Maity, A.; Pillay, K. Single stage batch adsorber design for efficient Eosin yellow removal by polyaniline coated ligno-cellulose. *Int. J. Biol. Macromol.* **2015**, *72*, 732–739. [CrossRef]
59. Alyasi, H.; Mackey, H.R.; Loganathan, K.; McKay, G. Adsorbent minimisation in a two-stage batch adsorber for cadmium removal. *J. Ind. Eng. Chem.* **2020**, *81*, 153–160. [CrossRef]

Disclaimer/Publisher's Note: The statements, opinions and data contained in all publications are solely those of the individual author(s) and contributor(s) and not of MDPI and/or the editor(s). MDPI and/or the editor(s) disclaim responsibility for any injury to people or property resulting from any ideas, methods, instructions or products referred to in the content.